3. REMOVAL OF ASSUMPTIONS

In the last section, the performance of the LOBD and various suboptimum nonlinearities (e.g., the hard limiter) was evaluated using the Central Limit Theorem in that only the mean and variance of the detection variable δ needed to be evaluated and also using the sufficiently small signal assumption to then evaluate the required integrals (6). We now want to remove these assumptions to see what effect they may have on estimating the performance of actual systems.

There are two possible approaches. The first is direct computer simulation to obtain Monte Carlo performance results comparing the various nonlinearities. The Middleton models are such that it would be difficult to rapidly generate the random noise samples required. The second approach is to use the Central Limit Theorem, but evaluate the integrals (6) directly without the small signal assumptions. This is also a formidable task, in general, due to the mathematical complexity of the noise models. There is one Class B situation, however, where both the above methods can be used. For Class B noise with $\alpha = 1$, Middleton (1976) has shown that the model (20) reduces to the following,

$$p_Z(z) \simeq \frac{2A_\alpha \sqrt{\Omega}}{\pi(4z^2 + \Omega A_\alpha^2)} \quad , \tag{25}$$

with the corresponding envelope APD given by

$$p(E > E_o) \simeq \frac{1}{\sqrt{1 + 4E_o^2/\Omega A_\alpha^2}} \quad . \tag{26}$$

The expressions above are models of the Hall (1966) type (Hall parameter $\theta = 2$), so the Middleton models can give some physical basis for the Hall model. The above [(25) and (26)] are only good approximations at the high amplitude "tails" and then only for relatively large values of $A_\alpha (A_\alpha \geq 1)$. Figure 4 shows the Hall model envelope distribution from (26) and the Middleton envelope distribution from (21) for $\alpha = 1$ and $A_\alpha = 1$. Also shown on Figure 4 is the Middleton model for $\alpha = 1$ and $A_\alpha = 10^{-3}$. As can be seen, the approximation given by (26) is only valid for large amplitudes and that (26) can be used to approximate the entire distribution only for the larger values of A_α. We are, of course, assuming that the physical-statistical model of Middleton is the appropriate model to "match" the actual environment (this has been reasonably well substantiated) and are using the Hall model

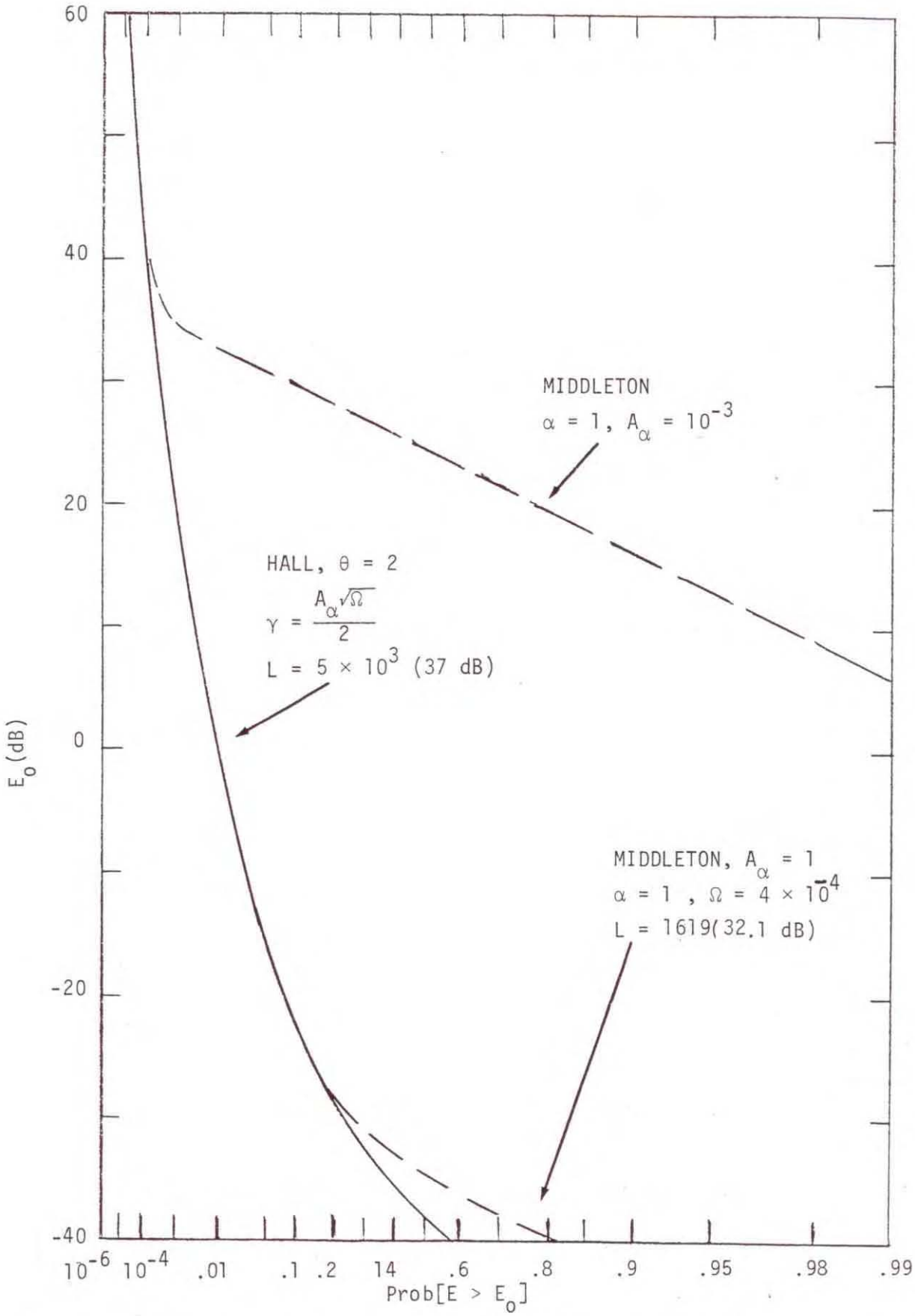

Figure 4. Comparison of the Middleton model for $\alpha = 1$ and $A_\alpha = 1$ and 10^{-3} with the Hall model, $\theta = 2$.

via (25) and (26) to obtain a simple mathematical form for a special case of Middleton's model.

For the Middleton model ($\alpha = 1$, $A_\alpha = 1$), L = 32.1 dB (Figure 2). The general Hall model has two parameters, θ and γ, and is given by

$$p_Z(z) = \frac{\Gamma\left(\frac{\theta}{2}\right)\gamma^{\theta-1}}{\Gamma\left(\frac{\theta-1}{2}\right)\sqrt{\pi}\left[z^2+\gamma^2\right]^{\theta/2}} \tag{27}$$

For $\theta = 2$ and $\gamma = A_\alpha\sqrt{\Omega}/2$, the Middleton approximation (25) is obtained. The corresponding general Hall APD form is

$$P[E > E_o] = \frac{\gamma^{\theta-1}}{\left(E_o^2+\gamma^2\right)^{(\theta-1)/2}} \quad . \tag{28}$$

When (27) is used in the "L integral" (8), we obtain

$$L = \frac{\theta^2\Gamma\left(\frac{\theta}{2}\right)\gamma^{\theta-1}}{\Gamma\left(\frac{\theta-1}{2}\right)\sqrt{\pi}} \int_{-\infty}^{\infty} \frac{z^2}{\left(z^2+\gamma^2\right)^{\frac{\theta}{2}+2}}\, dz \quad . \tag{29}$$

The parameter γ is a "normalizing parameter" equivalent to Ω in the Middleton model. For our case ($\alpha = 1$, $A_\alpha = 1$), $\gamma = \sqrt{\Omega}/2$. For $\theta = 2$, (29) then gives

$$L = 2/\Omega \quad . \tag{30}$$

The parameter Ω is defined as $2/(\text{envelope rms})^2$ (since the envelope power is twice the actual noise power), and the envelope rms must be computed from the model. In obtaining the results of Figure 2, the Middleton model was assumed to saturate at 80 dB above the Gaussian level or at an exceedance probability of 10^{-6}, whichever came first. That is, we must use a truncated model since the rms for the actual model does not exist. For the Middleton model ($A_\alpha = 1$, $\alpha = 1$), this gives $\Omega = 3.99959 \times 10^{-4}$. For the corresponding Hall model (for any large truncation point), we obtain for $\theta = 2$ and truncation at 80 dB, corresponding to the Middleton example,

$$0.5 \times (\text{Envelope rms})^2 = \frac{1}{2}\gamma \int_0^{10^4} \frac{E^2}{(E^2 + \gamma^2)^{3/2}}\, dE = 1 , \qquad (31)$$

or $$\gamma = \sqrt{2} \times 10^{-2} ,$$

resulting in [from (26) and (28)] $\Omega = 4 \times 10^{-4}$, almost precisely the normalization value obtained earlier for the Middleton example. Therefore, for the Hall model, $\theta = 2$, properly normalized, $L = 5 \times 10^3$ or 37 dB. For the Middleton example, $L = 32.1$ dB and for the corresponding Hall model, $L = 37$ dB even though the impulsive tails are essentially identical. This points out that the value of L depends on the relationship between the low level Gaussian portion of the distribution and the rms level of the entire distribution. As can be seen from Figure 4, when the two distributions are "matched," the Hall distribution has a "lower" Gaussian level, resulting in a somewhat larger L. From now on, we will restrict our attention to (26), $L = 37$ dB (or $\Omega = 4 \times 10^{-4}$).

By using (25) for our pdf of the interfering noise, the integrals (6) can be directly integrated with no small-signal assumption. We obtain from (6) and (25)

$$E[y_i|H_1] = \frac{\sqrt{\Omega}}{\pi} \int_{-\infty}^{\infty} \frac{z}{\left(z^2 + \frac{\Omega}{4}\right)\left[\left(z - S_{1i}\right)^2 + \frac{\Omega}{4}\right]}\, dz , \qquad (32)$$

and

$$E[y_i^2|H_1] = \frac{2\sqrt{\Omega}}{\pi} \int_{-\infty}^{\infty} \frac{z^2}{\left(z^2 + \frac{\Omega}{4}\right)^2\left[\left(z - S_{1i}\right)^2 + \frac{\Omega}{4}\right]}\, dz . \qquad (33)$$

The two integrals are most easily evaluated by contour integration using residues. After a rather extensive amount of algebra, we obtain

$$E[y_i|H_1] = \frac{2S_{1i}}{S_{1i}^2 + \Omega} \quad , \tag{34}$$

and

$$E[y_i^2|H_1] = \frac{2(3S_{1i}^2 + \Omega)}{(S_{1i}^2 + \Omega)^2} \quad , \tag{35}$$

so that

$$Var[y_i|H_1] = \frac{2}{S_{1i}^2 + \Omega} \quad . \tag{36}$$

Therefore, for the detection variable δ (Figure 1),

$$E[\delta|H_1] = -E[\delta|H_2] = 4 \sum_{i=i}^{N} \frac{S_{1i}^2}{S_{1i}^2 + \Omega} \quad , \tag{37}$$

and

$$Var[\delta|H_1] = Var[\delta|\ H_2] = 8 \sum_{i=1}^{N} \frac{S_{1i}^2}{S_{1i}^2 + \Omega} \quad . \tag{38}$$

Of course, for $S \to 0$, the above (37) and (38) reduce to the results obtained earlier (10) ($\Omega = 2/L$ and $LS << 1$).

The hard-limiter result obtained earlier (19), that is

$$L_{eff} = 4p_Z^2(0) \quad , \tag{39}$$

is a limiting result ($S \to 0$). For the Hall approximation (25)

$$L_{eff} = \frac{16}{\pi^2 \Omega} = 0.81\ L, \tag{40}$$

so for the Hall model the hard-limiter, according to (40), will result in 0.912 dB degradation, while for the corresponding Middleton model, the hard-limiter (in the limit) will result in a 1.5 dB degradation (Figure 2).

In terms of the actual signal samples, the suitably small signal approach gives

$$E[y_i|H_1] \doteq -2\, p_Z(0)\, S_{1i} \ , \tag{41}$$

so that for the detection variable δ,

$$E[\delta|H_1] = -E[\delta|H_2] \doteq \frac{8}{\pi\sqrt{\Omega}} \sum_{i=1}^{N} S_{1i}^2 \ , \tag{42}$$

and

$$Var[\delta|H_{1,2}] \doteq 4 \sum_{i=1}^{N} \left(S_{1i}^2 - \frac{16}{\pi^2\Omega} S_{1i}^4 \right) \ .$$

Without this small-signal assumption, the integrals (6) eventually give,

$$E[\delta|H_1] = E[\delta|H_2] = \frac{4}{\pi} \sum_{i=1}^{N} S_{1i}\, \mathrm{Tan}^{-1} \left(\frac{2\, S_{1i}}{\sqrt{\Omega}} \right) , \tag{43}$$

and

$$Var[\delta|H_{1,2}] = 4 \sum_{i=1}^{N} \left\{ S_{1i}^2 - \frac{4}{\pi^2} S_{1i}^2 \left[\mathrm{Tan}^{-1} \left(\frac{S_{1i}}{\sqrt{\Omega}} \right) \right]^2 \right\} .$$

Of course, as before as $S \to 0$, the results (43) approach those of (42). Also note that in (42) the variance quickly becomes negative as S increases, but in (43) the variance exists for all signal levels (but $\to 0$ as $S \to \infty$).

For the signaling set given by (12), we can generate our signal samples as follows:

$$S_1(t_i) = S_{1i} = \sqrt{2S} \cos \left[\frac{Q}{N-1} \cdot (i - 1) \right] \ , \tag{44}$$

where

$$t_i = \frac{T}{N-1} (i - 1) \qquad \text{and} \qquad Q = \omega_0 T \ .$$

We now use (44), (37,38), (42), or (43) in (11) to estimate performance for various signal-to-noise ratios S and number of samples N. (Also, for the coherent case considered here, it is just as valid to make all the signal samples the same, namely, $s_{1i} = \sqrt{S}$. In fact, this was done for the computer Monte Carlo simulations covered next.)

The comparison of the results using (44), (43), and (42) for N = 100 are shown in Figure 5. On Figure 5, three curves are given: the standard result ($S \to 0$) from (13,14), the result using (37,38) ($S \not\to 0$), and the hard limiter result from (43) ($S \not\to 0$). The signal samples were generated via (44). Also shown on Figure 5 are simulation results (to be covered in the next section) for the LOBD nonlinearity (bandpass) and the bandpass limiter, and we see that the calculated results are quite close to the simulated results in all cases. Note that removing the small signal assumption makes only about 1.5 dB difference (the same is true for the hard-limiter). Since N = 100 here, we expect the Central Limit Theorem approximation to be quite adequate, and we see that it is.

Figure 6 shows results for N = 10. First, we note that performance cannot be calculated from the normal result (13,14) since the variance quickly becomes negative. This is noted by the dashed curve ($S \to 0$). The hard-limiter calculation from (43) ($S \not\to 0$) matches the simulation results only for small signal levels and departs rapidly as the signal increases. The LOBD calculated results from (37,38) ($S \not\to 0$) follow the simulated results better. The differences are, of course, due to the Central Limit Theorem approximation used for the calculated results not being valid for N = 10, especially in the "tails." The most interesting result shown, however, is that the hard-limiter outperforms the LOBD as the signal level increases (around SNR = -28 dB and $P_e = 10^{-6}$ in this case). Even though N = 10 and the simulation results go to $P_e = 10^{-6}$, the simulation results shown are statistically quite accurate. That is, the effect shown is real.

4. MONTE CARLO COMPUTER SIMULATION RESULTS

In the previous section, the assumption of suitably small signal normally used in performance estimation was removed for one Class B example. However, the Central Limit Theorem argument was still required. The only way to get around this, since it is impossible to find the actual pdf of the detection variable δ instead of just its mean and variance, is by direct computer simulation. This means that we must be able to quickly generate a large number of random samples from the appropriate noise and signal distributions. For example, if N = 100 and we want to determine performance in the range $P_e = 10^{-6}$ and we decide that we need at least ten

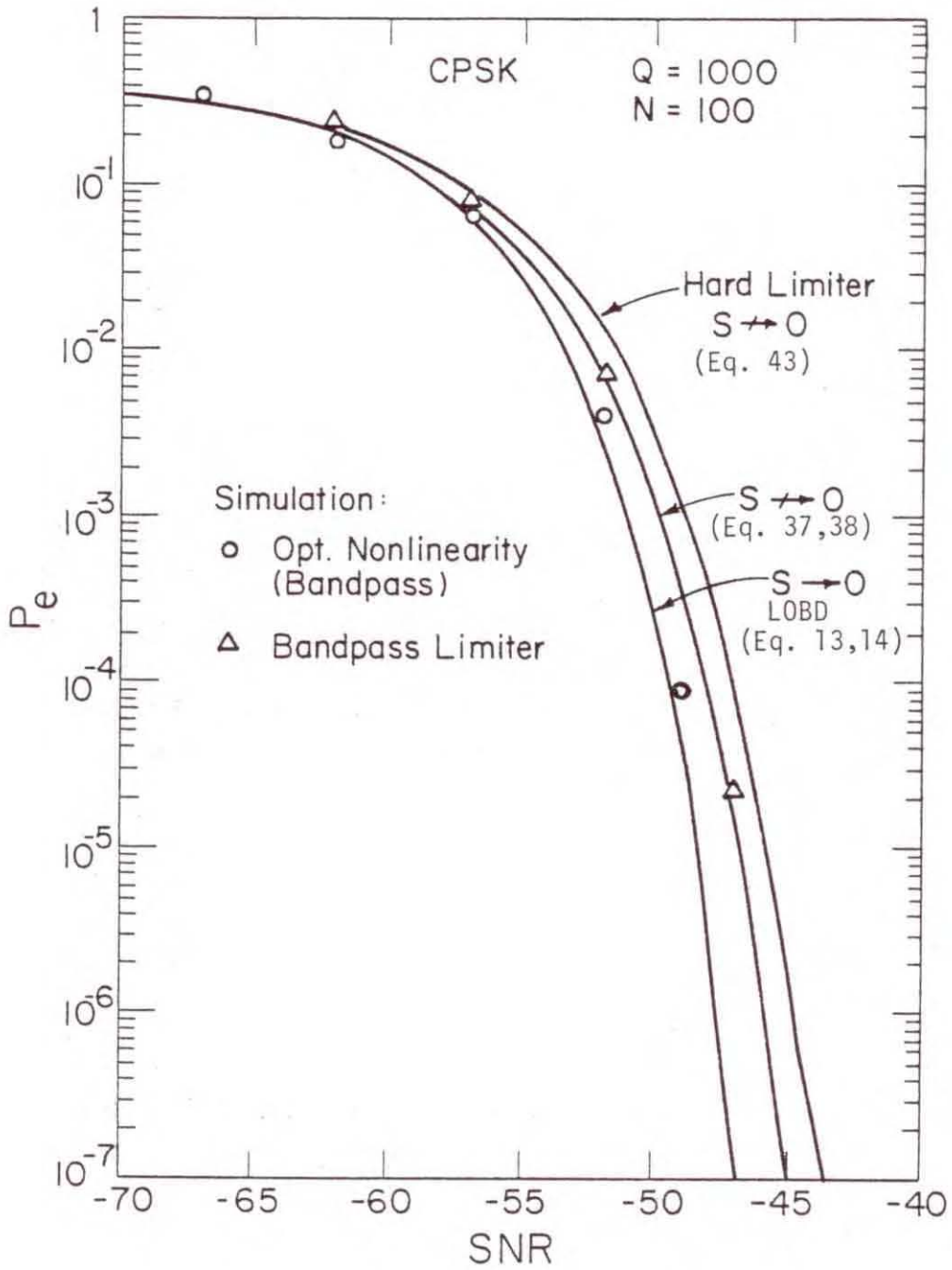

Figure 5. Calculated and simulation results for the hard-limiter and LOBD nonlinearities for N = 100.

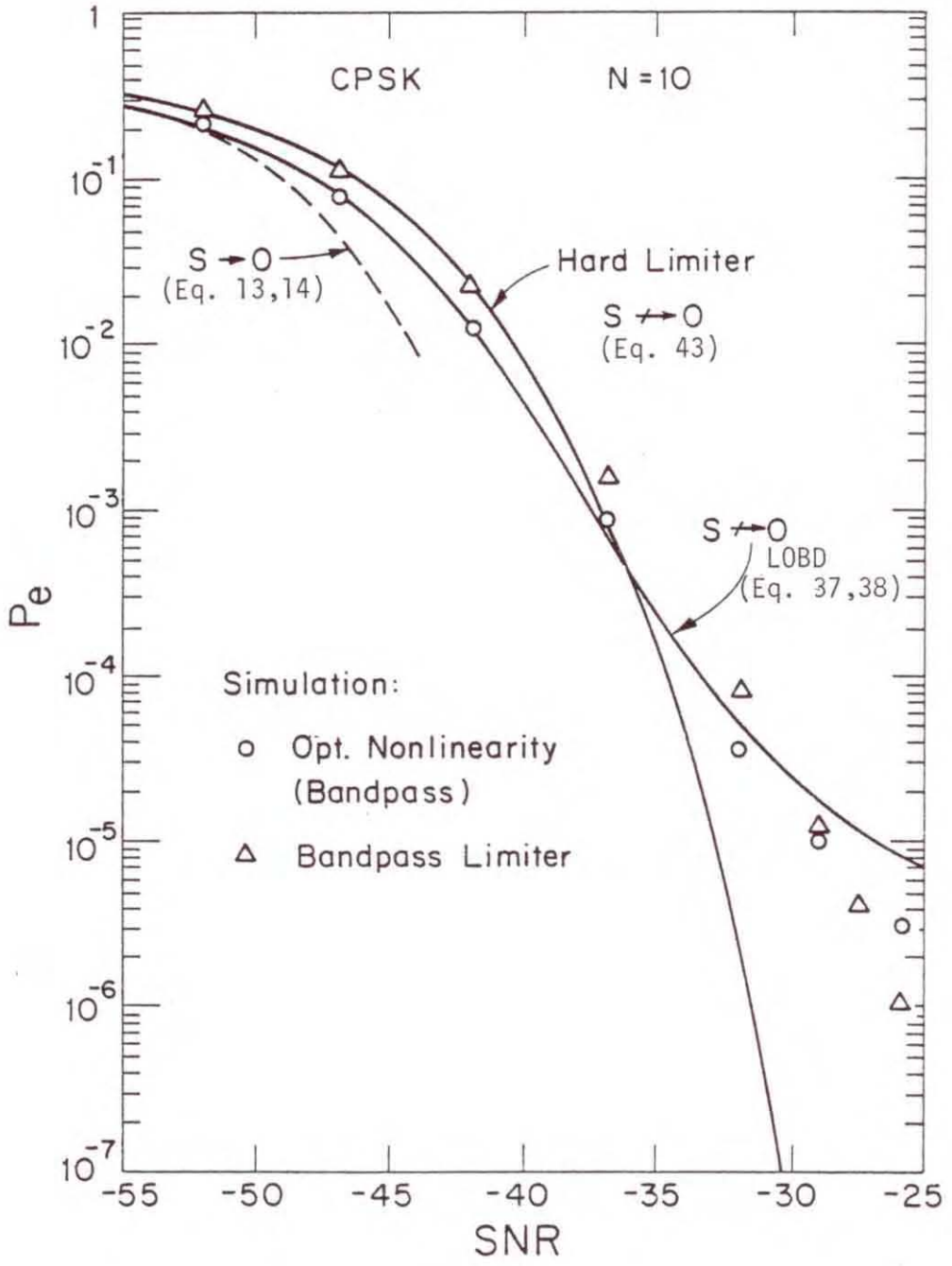

Figure 6. Calculated and simulation results for the hard limiter and LOBD nonlinearities for N = 10.

errors for statistical significance, then we need $100 \times 10 \times 10^6 = 10^9$ random samples for this one point. This problem of the large number of random samples required has always been one of the drawbacks of Monte Carlo simulation, and, obviously, the use of Middleton's model to generate random interference samples is out of the question without resorting to some much simpler approximation. It turns out that it is reasonably efficient to generate random noise samples from the Hall model.

In using Monte Carlo simulation, the accuracy of the estimate must be specified and this then usually determines the number of random samples required. A simple explanation of the Monte Carlo concept and various techniques has been given long ago by Kahn and Mann (1957) and an excellent survey has been presented by Halton (1970). Halton especially covers the important area of "variance reduction." The variance reduction technique appropriate to our problem is termed "Importance Sampling." The general idea of importance sampling is to draw samples from a distribution other than the one given by the problem and to carry along an appropriate weighting factor, which, when multiplied into the final results, corrects for having the wrong distribution. The biasing is done in such a way that the probability of the samples being drawn from an "interesting" region is increased. If good Importance Sampling techniques can be developed for a problem, then many less (orders of magnitudes less) random samples are required to achieve the same given level of statistical significance. Unfortunately, it is usually difficult to develop such techniques. A detailed example of using Importance Sampling quite effectively for nonlinear channels and Gaussian noise has been given by Shanmugam and Balaban (1980). Although substantial effort was expended, we could not develop any significantly "good" sampling methods for our problem at hand so that the results presented in this section are based on straight Monte Carlo techniques.

In generating the random samples in order to obtain the input x_i (Figure 1) to the system being simulated, bandpass processes are employed. That is, envelope and phase representations are used as in Figure 7. In Figure 7, the signal sample is $\sqrt{S}$, corresponding to the signals given by (12). Because of symmetry only $S_1(t)$ ($\sqrt{S}$) needs to be "sent." An error will occur whenever the resultant $\overline{X}_i$, after modification by the nonlinear receiver, lies in the shaded region of Figure 7. Actual detection is based on the sum of N such signal plus noise resultants. For a constant signal, all signal samples are the same, namely, the $\sqrt{S}$. Flat fading signal situations are obtained by using a constant signal throughout a detection interval T, but then allowing this "constant" to vary from one detection interval to the next according to some fading distribution. Results for flat Rayleigh fading

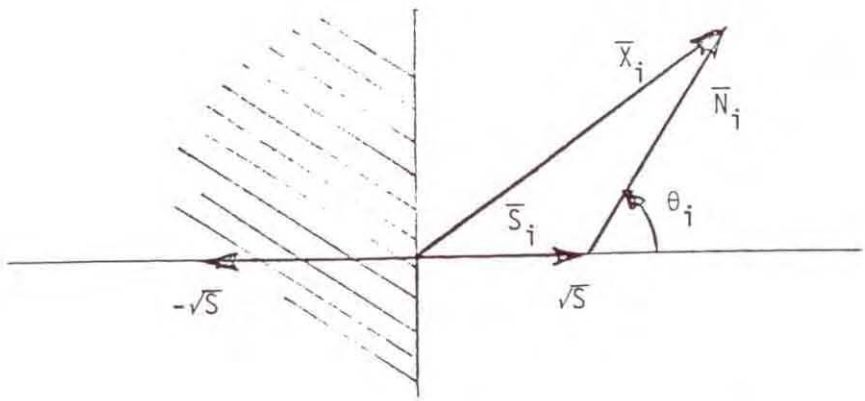

Figure 7. Signal phasors plus noise phasor for CPSK.

signals will be included here. Other fading situations can be simulated by allowing the signal samples to vary within a detection interval. On Figure 6, each noise sample $\overline{N}_i$ is obtained from the appropriate envelope (e.g., Rayleigh for Gaussian noise) and each noise phase angle, θ_i, is obtained from a uniform distribution $0 \leq \theta < 2\pi$.

The details of generating random samples from arbitrary distributions is treated by Bogdan (1981). The procedures start by generating a random sample (or samples) from a uniform distribution in the interval (0,1] and then modifying this sample according to the desired distribution. To do this usually requires taking the inverse of the cumulative distribution function (which, of course, makes it impossible to use Middleton's model). For example, for Gaussian noise, Rayleigh envelope, if V is uniform on (0,1], then a Rayleigh distributed random variable, X, is obtained from

$$X = [-2\,\sigma^2\,\ell n\,(1 - V]^{1/2}\,, \tag{45}$$

where σ^2 is the real noise power. If we have normalized the noise envelope to its rms value, i.e., envelope power = 1, then the real noise power, σ^2, is 1/2. For the Hall model, random samples are obtained from

$$X = \gamma(V^{\frac{-2}{\theta-1}} - 1)^{1/2}\,, \tag{46}$$

and we will give results for $\theta = 2$ (as in the last section) and for $\theta = 4$. Also, for the Hall model, the LOBD nonlinearity is quite simple (see Figure 1),

$$y_i = \frac{\theta x_i}{x_i^2 + \gamma^2} \quad . \tag{47}$$

In actual systems, the nonlinearity (47) operates on the magnitude of the complex received waveform sample, that is, the magnitude of $\overline{X}_i$ is used. In the hard limiter case, the bandpass version becomes a bandpass limiter. Physically, the bandpass limiter is a hard limiter followed by a zonal filter, so that no signal distortion is obtained from the nonlinearity and the following correlation receiver remains "matched" to the signal, as in the previous analysis. The behavior of the bandpass limiter when used with Gaussian noise and one CW signal has been analyzed in great detail by Davenport (1953) (see also problem 13, page 311 of Davenport and Root, 1958). A simplified analysis has also been given by Cahn (1961). This analysis shows that, in terms of signal-to-noise ratios (SNR) in and out of the nonlinearity.

$$\left(\frac{S}{N}\right)_o = \frac{\pi}{4}\left(\frac{S}{N}\right)_I \qquad \text{when } \left(\frac{S}{N}\right)_I << 1 \, ,$$

and (48)

$$\left(\frac{S}{N}\right)_o = 2\left(\frac{S}{N}\right)_I \qquad \text{when } \left(\frac{S}{N}\right)_I >> 1 \, .$$

That is, Gaussian noise and the bandpass limiter results in 1.05 dB degradation for small S/N and 3 dB degradation for large S/N. Using (19) to obtain L_{eff} for the hard-limiter and Gaussian noise, we obtain $L_{eff} = \pi/2 = 1.57$, or 1.96 dB degradation.

The receiver structures that were simulated are shown in Figure 8. The bandpass receivers (a,b,d, Figure 8) were used almost exclusively, but some results for the others (c and e, Figure 8) were obtained, mainly for curiosity's sake and to see how much difference resulted.

If the actual probability of error is P_e, then an estimate of P_e is

$$\hat{P}_e = \frac{1}{K} \sum_{i=1}^{K} a_i \, , \tag{49}$$

where a_i is 1 if the i^{th} transmitted symbol is in error and zero otherwise and K is the number of transmitted symbol with detection based on N sample points for each of the K symbols. The mean and variance of $\hat{P}_e$ are given by P_e and $P_e(1 - P_e)/K$,

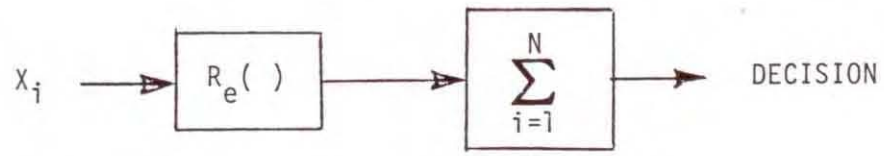

a) Linear Correlator Receiver

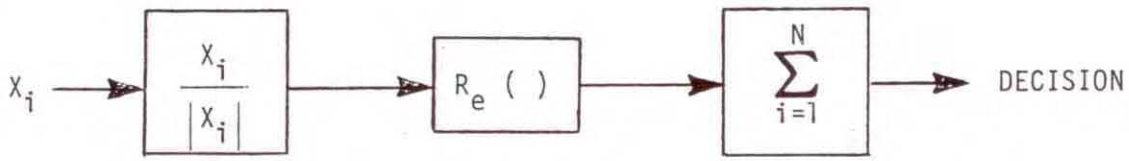

b) Bandpass Limiter Receiver

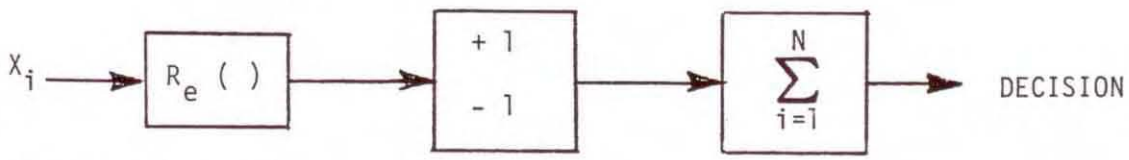

c) Hard-Limiter Receiver

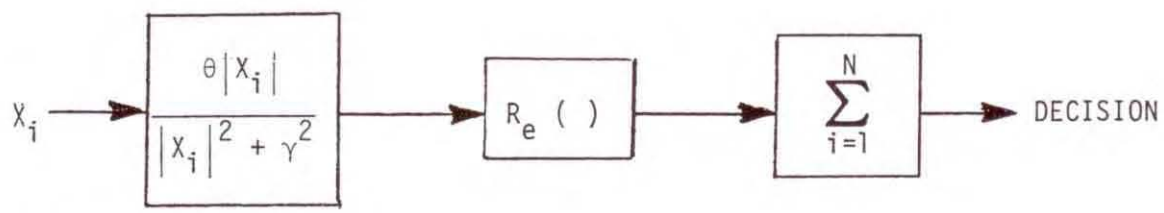

d) LOBD Bandpass Receiver

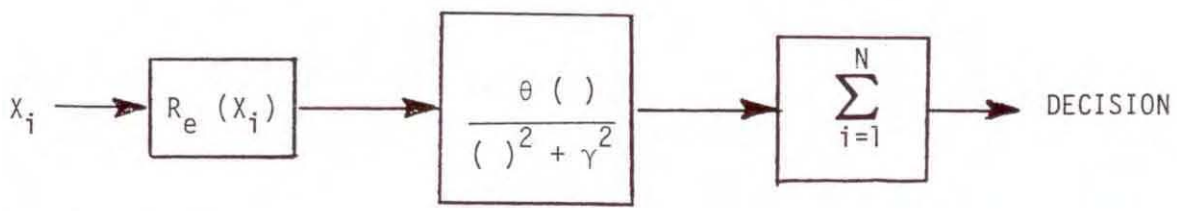

e) LOBD Receiver

Figure 8. Receiver structures.

respectively. For low probability of error, the normalized standard deviation is approximately $(KP_e)^{-1/2}$. The simulation programs are designed so that either a maximum number of symbols transmitted or a minimum number of errors detected will terminate the execution.

The first simulation results are given on Figure 9. These are for Gaussian noise for N = 1,10,100 using a linear receiver (optimum) and the hard-limiter [(c) of Figure 8] and the bandpass limiter. The object here is to make sure that the simulation results correspond to the known theoretical results so that we know the simulation programs are functioning properly. Results for a Rayleigh flat fading signal and Gaussian noise are also given on Figure 9 (N = 1). As expected, we see that the "hard limiter" is slightly inferior to the bandpass limiter.

Figure 10 shows results using the Hall model ($\theta = 2$) "normalized" as in the previous section to represent Middleton's model. The result from Figure 10 for N = 10 and 100 were discussed in the last section where they were compared to various analytical results. Note the interesting results for the linear receiver. Identical results were obtained for N = 1, 10, and 100. This is, of course, not physically meaningful and is the result of using a model for which the moments do not exist. This "infinite power" problem goes away whenever a nonlinearity is employed, as with the other results of Figure 10. For a linear receiver, for N = 10 say, detection is based on a "noise sample" which is the sum of the ten noise samples from the basic underlying distribution. Except for Gaussian noise, the distribution of the "sum sample" is different from the distribution of each individual sample, and approaches Gauss via the Central Limit Theorem. This makes it difficult to analytically determine the performance of linear systems in non-Gaussian noise for time bandwidth products other than 1. The above is for "real" noise processes with finite moments. Consider the Hall model for $\theta = 2$. The pdf is given by

$$p_Z(z) = \frac{\gamma}{\pi(z^2 + \gamma^2)} \quad , \tag{50}$$

so that the characteristic function is

$$\phi_Z(u) = \int_{-\infty}^{\infty} e^{-uz} \frac{\gamma}{\pi(z^2 + \gamma^2)} \, dy \tag{51}$$

This gives

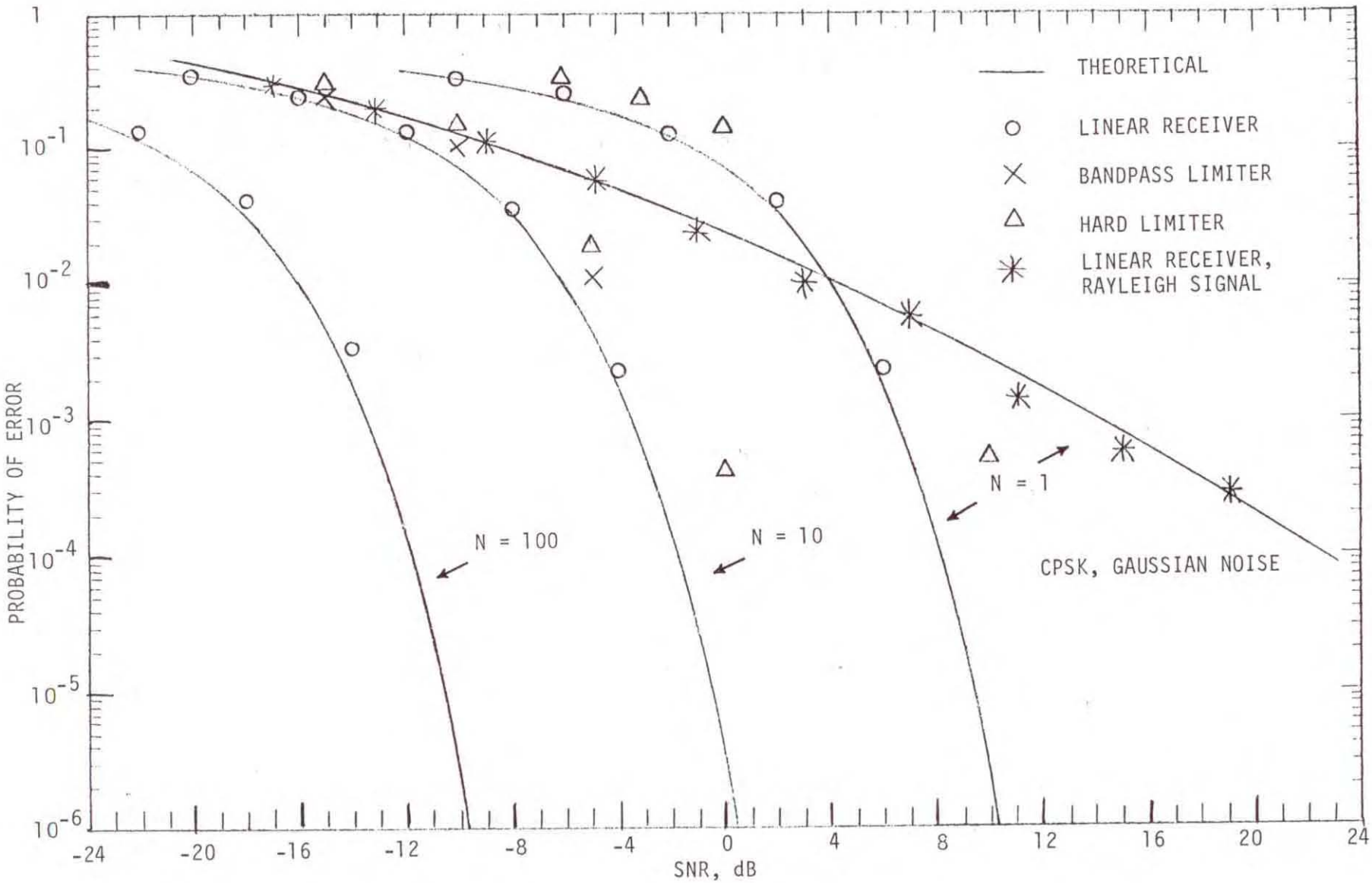

Figure 9. Simulation results with Gaussian noise for Rayleigh fading and constant signal for binary CPSK.

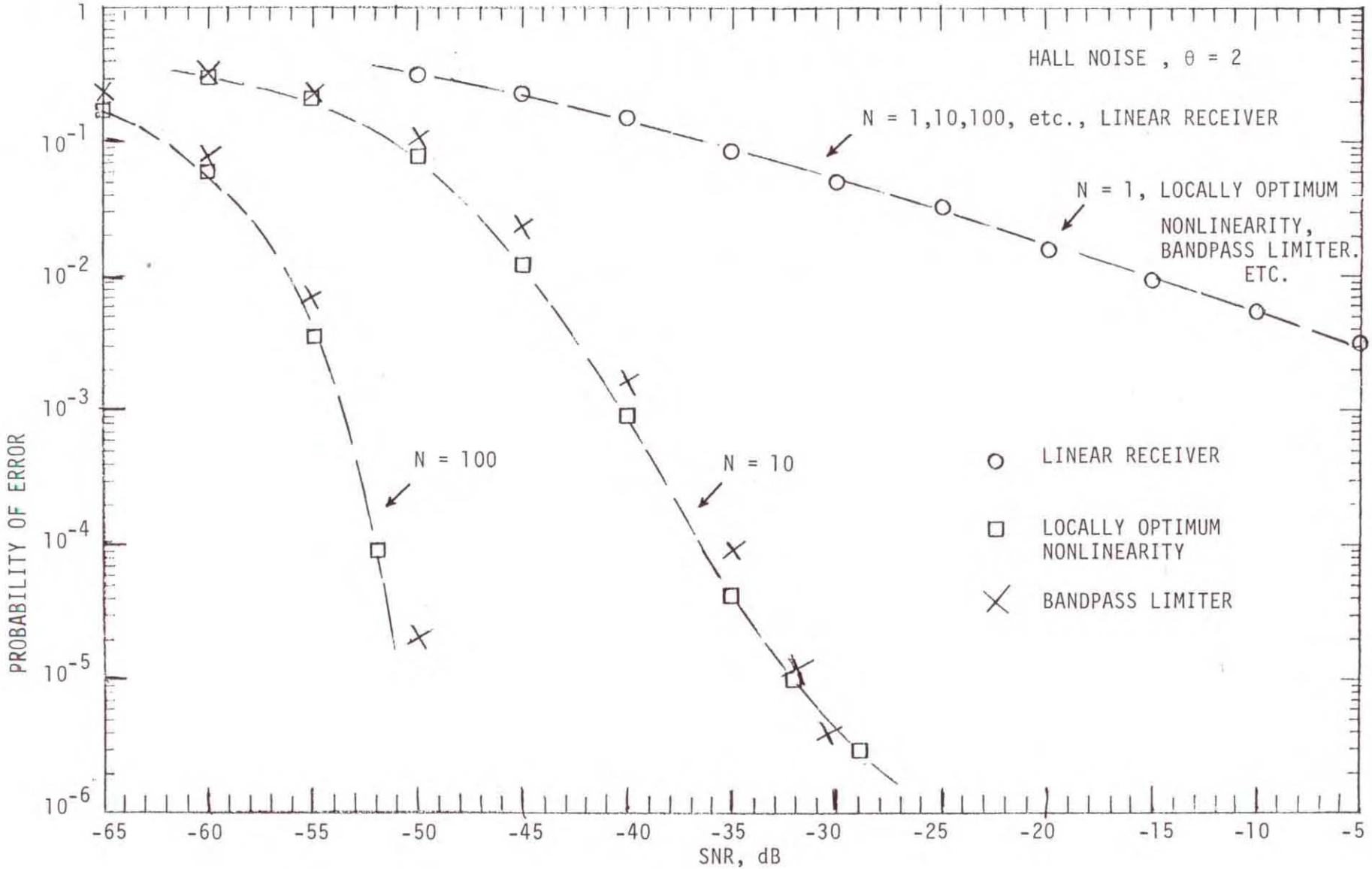

Figure 10. Simulation results with Hall noise, θ = 2, and constant signal.

$$\phi_Z(u) = \frac{2\gamma}{\pi} \int_0^\infty \frac{\gamma}{(y^2 + \gamma^2)} \cos uz \, dz = e^{-\gamma u} \quad . \tag{52}$$

So if

$$Y = \sum_{i=1}^{N} Z_i \quad , \tag{53}$$

the pdf of Y is given by

$$p_Y(y) = \frac{N\gamma}{\pi \left[y^2 + (N\gamma)^2 \right]} \quad . \tag{54}$$

That is, Y has the same pdf as the individual Z_i's, but is N times "bigger." This explains the linear receiver results of Figure 10. In doing the simulation with $\theta = 2$ and the linear receiver, a truncated Hall model was also used. That is, all values generated that were larger than some threshold were either discarded or reduced to the threshold value. This procedure made no difference and the same results shown on Figure 10 were obtained. That is, the mathematics given above still dominated. Also indicated on Figure 10 for N = 1 are results using the LOBD nonlinearity and the bandpass limiter. As indicated, these results were essentially identical to those obtained for the linear receiver, demonstrating the known result that for N = 1, no improvement can be obtained by using nonlinear receivers and in order for nonlinearities to be effective, N must be greater than 1.

Figure 11 gives simulation results for the Hall, $\theta = 2$, noise and a Rayleigh fading signal, N = 10. Note that as for a constant signal and N = 10 (Figure 6 and 10), the bandpass limiter outperforms the LOBD nonlinearity as the SNR increases. This behavior is easier to see for a Rayleigh signal, since the P_e's are much higher at the "crossover" point between the LOBD and the bandpass limiter.

To complete the simulation results for $\theta = 2$, Figure 12 shows what happens when Gaussian noise is the actual interference and our receiver uses the LOBD nonlinearity for $\theta = 2$. The solid curve is the theoretical performance for the linear receiver in Gaussian noise (optimum) and the degradation caused by using the LOBD nonlinearity (N = 10) is shown. Using (16) and (17) to compute L_{eff}, we obtain the integrals

$$L_1 = \frac{-2\theta}{\sigma^2\sqrt{2\pi\sigma^2}} \int_{-\infty}^{\infty} \frac{2}{z^2 + \gamma^2} \, e^{-z^2/2\sigma^2} \, dz \quad ,$$

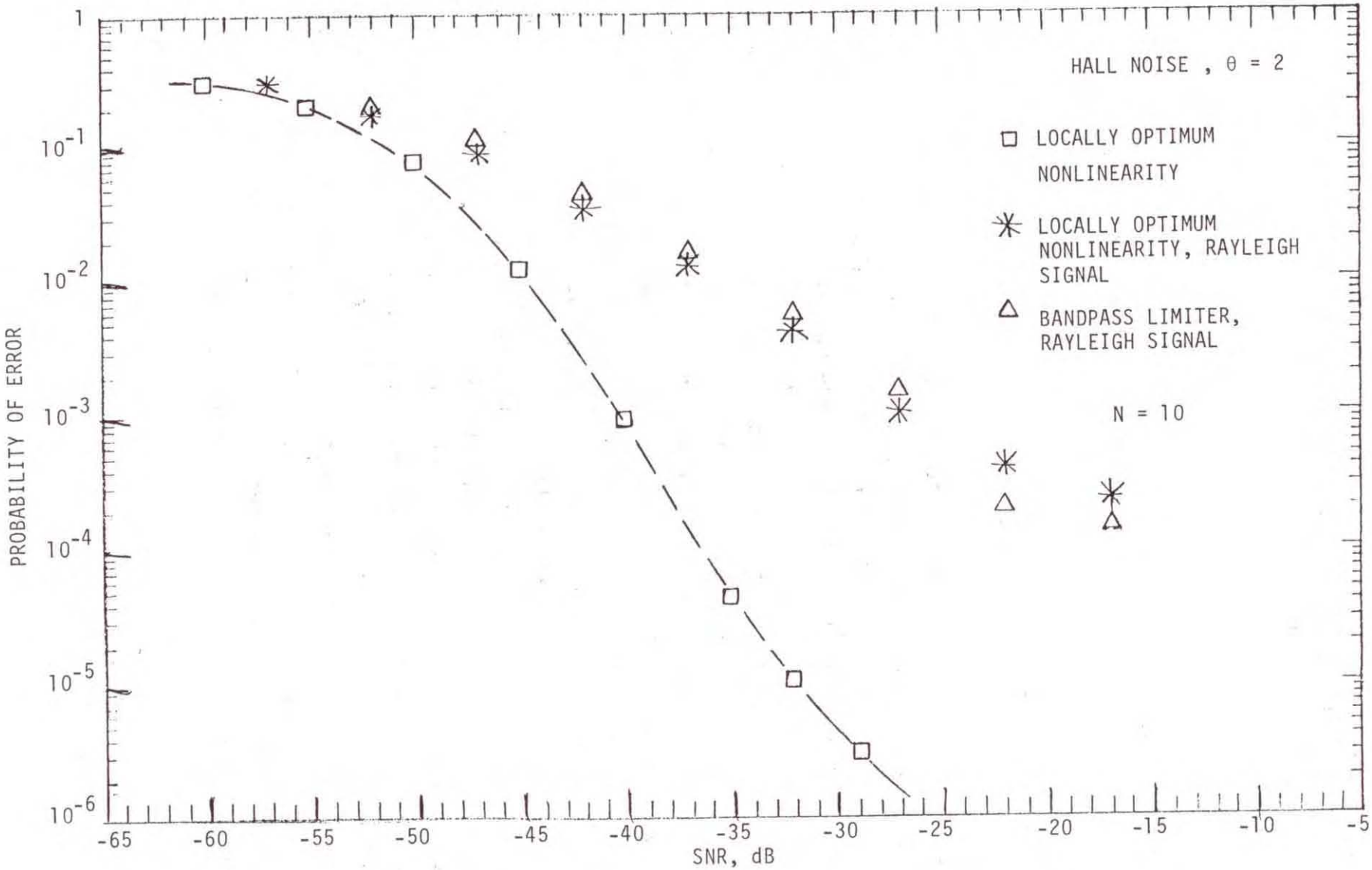

Figure 11. Simulation results for constant and Rayleigh fading signal, Hall noise, $\theta = 2$ and $N = 10$.

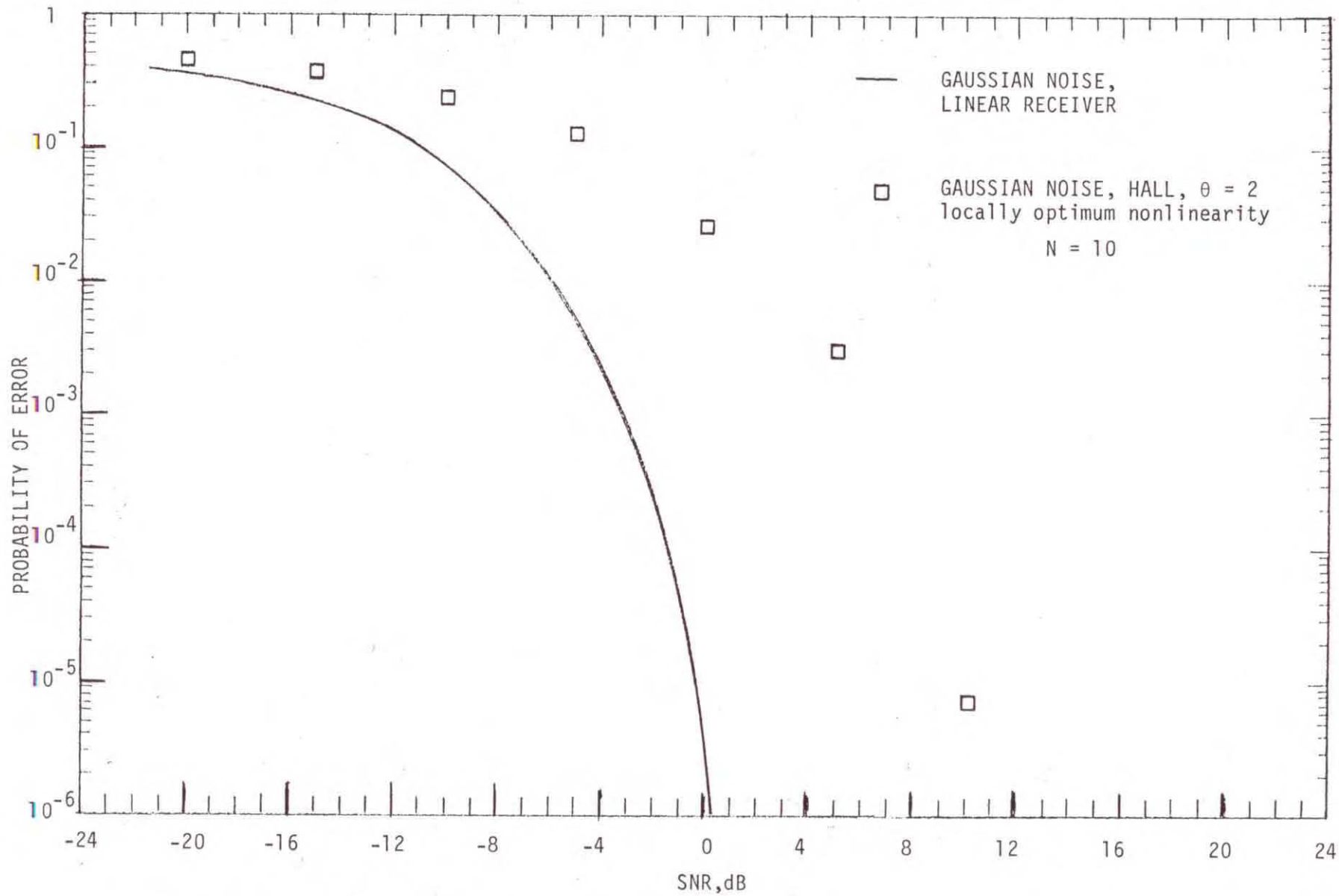

Figure 12. Simulation results for Gaussian noise into the LOBD, Hall θ = 2, nonlinearity.

and (55)

$$L_2 = \frac{2\theta^2}{\sqrt{2\pi\sigma^2}} \int_{-\infty}^{\infty} \frac{z^2}{z^2 + \gamma^2)^2} e^{-z^2/2\sigma^2} dz \quad .$$

The L_1 integral can be evaluated analytically but the L_2 apparently cannot be. Numerical integration of L_1 and L_2 gives

$$L_{eff} = L_1^2/L_2 = 0.0316 = -15.0 \text{ dB} \quad . \tag{56}$$

The L_{eff} tells us the degradation expected for "small" $S(>0)$ and $N \to \infty$. The degradation obtained for N = 10 using the simulation results is on the order of 10 dB from Figure 12. Simulation results for N = 100 were not obtained.

As detailed in Section 3, the Hall model, $\theta = 2$, properly normalized was used to approximate Middleton's model to "check" previous results based on suitably small signal and Central Limit Theorem arguments. Simulation results were also obtained for another Hall distribution, $\theta = 4$. Unlike the $\theta = 2$ case, the first three moments exist for the $\theta = 4$ case. The pdf for $\theta = 4$ is

$$p_Z(z) = \frac{2\gamma^3}{\pi(z^2 + \gamma^3)^2} \quad , \tag{57}$$

and the APD is

$$\text{Prob} \quad E > E_o = \frac{\gamma^3}{(E_o^2 + \gamma^2)^{3/2}} \quad . \tag{58}$$

If this is normalized to the envelope rms level (which now can be computed), then $\gamma = \sqrt{2}/2$. A quite interesting result is that for the Hall model, $\theta = 4$, the "improvement factor" L is only 4 (6 dB). Figure 13 shows the APD ($\theta = 4$) and this noise is obviously highly non-Gaussian. Comparing Figure 13 ($\theta = 4$) and Figure 4 ($\theta = 2$ and for which L = 37 dB), the noise distributions do not appear to be "all that much different," especially in the tails. Yet for $\theta = 4$, L is only 6 dB. As we will see from the simulation results, this "31 dB difference" (37-6) is quite real.

First, Figure 14 shows results for a linear receiver for both constant and Rayleigh fading signal. Since we are now using a "real" noise process with finite moments, we obtain "normal" results for the different time-bandwidth products. As

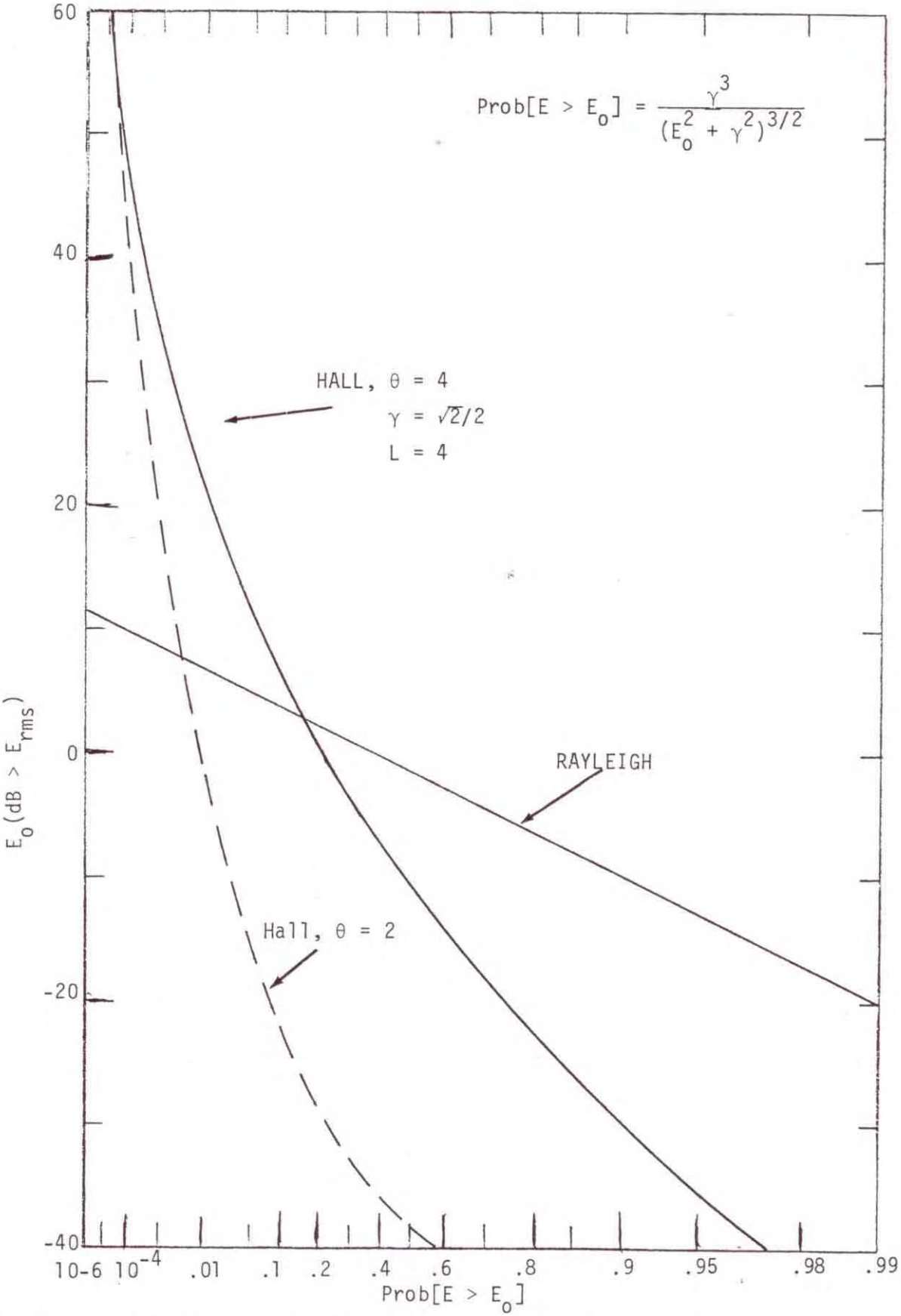

Figure 13. The Hall model APD for θ = 4. The APD is normalized to the rms envelope level.

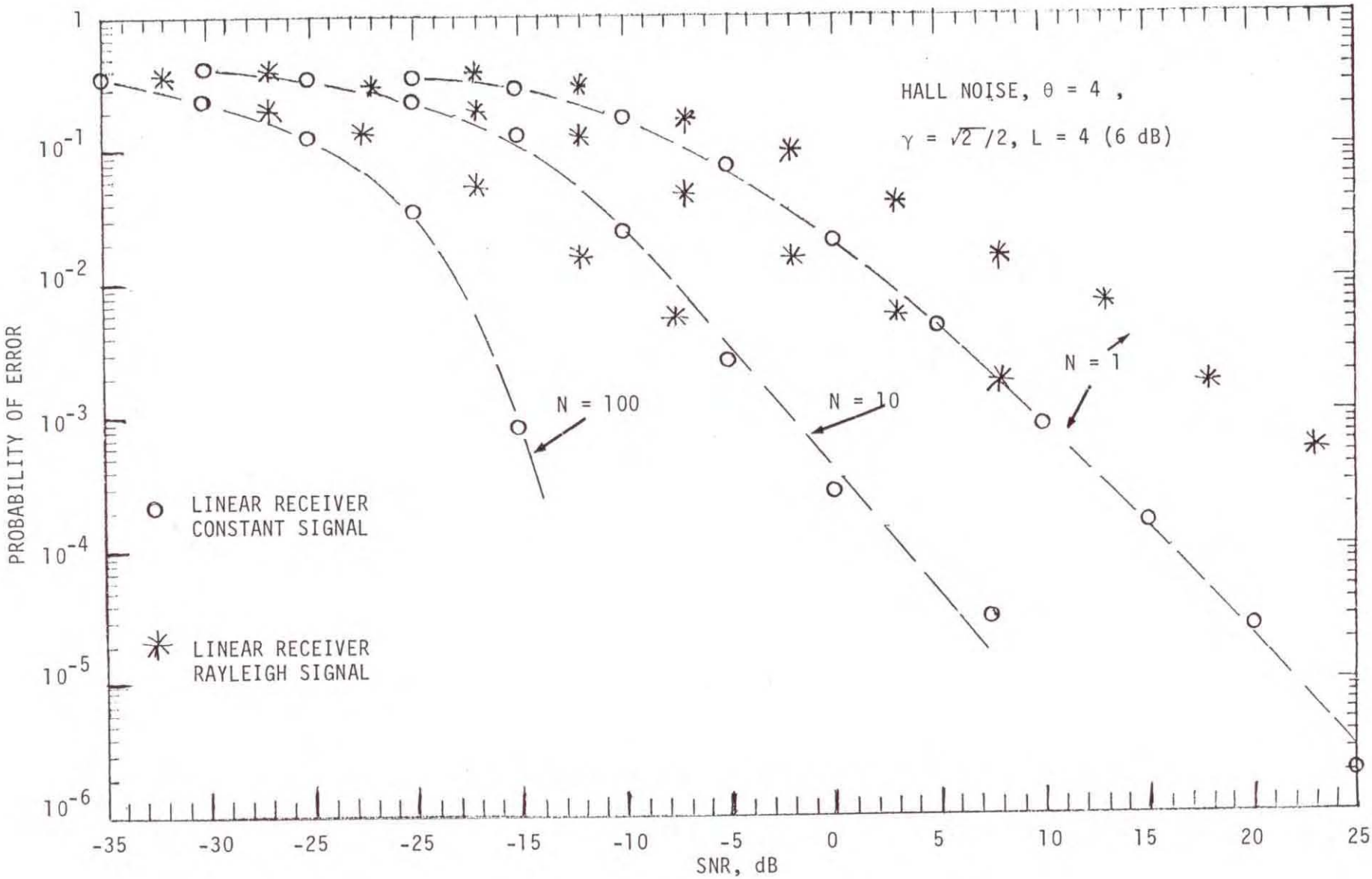

Figure 14. Simulation results for Hall noise θ = 4, and a linear receiver for both constant and Rayleigh fading signal.

Figure 14 shows, as N increases, the performance results look more and more like the standard result for Gaussian noise due to the Central Limit Theorem (which, as noted earlier, only applies to random variables with finite moments).

Figure 15 shows the linear receiver, constant signal, results along with results for the bandpass limiter and the LOBD nonlinearity. First, note that as before, use of nonlinearities for N = 1 gives no improvement over the linear receiver, but, of course, does give improvement for N = 10 and 100. For N = 100, this improvement is only 6 dB, as predicted by L. Note that the LOBD nonlinearity here also is only slightly superior to the bandpass limiter. From Figure 9 for N = 100, the linear receiver operating in Gaussian noise (optimum) requires approximately a SNR of -13 dB for $P_e = 10^{-3}$ and from Figure 15 the LOBD receiver (locally optimum) requires approximately -20 dB SNR for $P_e = 10^{-3}$. This is a 7 dB difference and the limiting difference predicted by L was 6 dB. Next, from Figure 10, N = 100, Hall $\theta = 2$ noise, a SNR of -53 dB is required for $P_e = 10^{-3}$. This is the "31 dB difference" (approximately) between the two Hall noises mentioned above and given by the two corresponding L values (37 dB versus 6 dB). This shows that we cannot arbitrarily say, by inspection, that a noise process which is "tremendously" non-Gaussian can result in "tremendous" improvement over the corresponding Gaussian or linear receiver situation.

Finally, Figure 16 compares performance for a constant signal and a Rayleigh fading signal for N = 10. Note, that while for the $\theta = 2$ case and N = 10, the bandpass limiter began to outperform the LOBD nonlinearity for both constant signal (Figures 6 and 10) and Rayleigh fading signal (Figure 11) as SNR increased. Here ($\theta = 4$) the LOBD nonlinearity appears to be "always" slightly superior to the bandpass limiter.

5. CONCLUSIONS AND DISCUSSION

In the derivation of the LOBD, two essential assumptions are made. That the desired signal is suitably small (see Middleton and Spaulding, 1983) and that the number of independent noise samples increases without limit. The usual means of estimating the performance, once the detectors have been derived, again make use of these two simplifying assumptions. This results in performance measures that are strictly true only in the limit. It has been the purpose here to investigate, via particular examples and computer Monte Carlo simulation, how the LOBD's will actually perform in actual possible operational situations. The results are varied, but in general, the "standard" limiting performance estimates do provide correct performance measures under appropriate conditions (large N and S sufficiently small).